

# Reinforcement Learning Control of a Biomechanical Model of the Upper Extremity

Florian Fischer, Miroslav Bachinski, Markus Klar, Arthur Fleig, Jörg Müller

University of Bayreuth, Bayreuth, Germany

## Abstract

We address the question whether the assumptions of signal-dependent and constant motor noise in a full skeletal model of the human upper extremity, together with the objective of movement time minimization, can predict reaching movements. We learn a control policy using a motor babbling approach based on reinforcement learning, using aimed movements of the tip of the right index finger towards randomly placed 3D targets of varying size. The reward signal is the negative time to reach the target, implying movement time minimization. Our biomechanical model of the upper extremity uses the skeletal structure of the *Upper Extremity Dynamic Model*, including thorax, right shoulder, arm, and hand. The model has 7 actuated degrees of freedom, including shoulder rotation, elevation and elevation plane, elbow flexion, forearm rotation, and wrist flexion and deviation. To deal with the curse of dimensionality, we use a simplified second-order muscle model acting at each joint instead of individual muscles. We address the lack of gradient provided by the simple reward function through an adaptive learning curriculum. Our results demonstrate that the assumptions of signal-dependent and constant motor noise, together with the objective of movement time minimization, are sufficient for a state-of-the-art skeletal model of the human upper extremity to reproduce complex phenomena of human movement such as Fitts' Law and the  $2/3$  Power Law. This result supports the idea that the control of the complex human biomechanical system is plausible to be determined by a set of simple assumptions and can be easily learned.

## Author summary

Among the infinite number of possible movements, humans are commonly assumed to choose those that optimize criteria such as minimizing movement time, subject to movement constraints such as signal-dependent and constant motor noise. The fact that these assumptions result in movements that exhibit characteristics of human movements has been shown in simplified models, such as point-mass models of the end-effector. Defining characteristics of human movements are the speed-accuracy trade-off described through Fitts' Law for aimed movements, and the  $2/3$  Power Law for curved movements. Here, we show that movement of a significantly more complex biomechanical model of the human upper extremity also exhibits these characteristics, when movement is learned via reinforcement learning under these simple assumptions.

## Introduction

Among the infinite number of movements that achieve a certain objective, such as reaching for a target, humans regularly choose movements that exhibit certain invariant

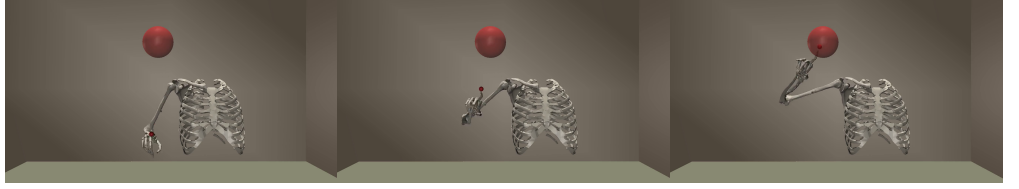


**Fig 1. Synthesized reaching movement.** A policy implemented as a neural network computes motor control signals of simplified muscles at the joints of a biomechanical upper extremity model from observations of the current state of the upper body. We use Deep Reinforcement Learning to learn a policy that reaches random targets in minimal time, given signal-dependent and constant motor noise.

characteristics. Aimed movements towards a spatially defined target exhibit a speed-accuracy trade-off described by Fitts’ Law [1]. Curved movements exhibit a relation between end-effector velocity and curvature described by the  $2/3$  Power Law [2, 3]. These phenomena have been shown to be a direct consequence of minimizing movement time, under signal-dependent and constant motor noise, in the case of simple end-effector models of the human hand [4]. Here, we aim to demonstrate that these simple assumptions are sufficient for a full skeletal upper extremity model to reproduce these phenomena of human movement. Our biomechanical model of the human upper extremity uses the skeletal structure of the *Upper Extremity Dynamic Model* by Saul et al. [5], including thorax, right shoulder, arm, and hand. The model has 7 actuated degrees of freedom (DOFs): shoulder rotation, elevation and elevation plane, elbow flexion, forearm rotation, and wrist flexion and deviation. While the thorax is fixed in space, the upper extremity can move freely by actuating these DOFs. To deal with the curse of dimensionality, following van Beers et al. [6], we use a simplified second-order muscle model acting at each DOF instead of individual muscles,

$$\begin{bmatrix} \sigma_{n+1}^{(q)} \\ \dot{\sigma}_{n+1}^{(q)} \end{bmatrix} = \begin{bmatrix} 1 & \Delta t \\ \frac{-\Delta t}{(t_e t_a)} & 1 - \Delta t \frac{t_e + t_a}{t_e t_a} \end{bmatrix} \begin{bmatrix} \sigma_n^{(q)} \\ \dot{\sigma}_n^{(q)} \end{bmatrix} + \begin{bmatrix} 0 \\ \frac{\Delta t}{t_e t_a} \end{bmatrix} c_n^{(q)}, \quad (1)$$

with model sampling interval  $\Delta t=2\text{ms}$  (controls are updated every 10ms), excitation and activation time constants  $t_e=30\text{ms}$  and  $t_a=40\text{ms}$ , respectively, and applied control  $c_n^{(q)}$  and resulting activation  $\sigma_n^{(q)}$  for each DOF  $q \in \mathcal{Q}$  (where  $\mathcal{Q}$  is the set of all DOFs), at time step  $n \in \mathbb{N}$ . We assume both signal-dependent and constant noise in the control, i.e.,

$$c_n^{(q)} = (1 + \eta_n) a_n^{(q)} + \epsilon_n, \quad (2)$$

where  $a_n = (a_n^{(q)})_{q \in \mathcal{Q}}$  denotes the action vector obtained from the learned policy and  $\eta_n$  and  $\epsilon_n$  are Gaussian random variables with zero mean and standard deviations as described by van Beers et al. [6]. The torques that are applied at each DOF independently are obtained from multiplying the respective activation  $\sigma_n^{(q)}$  with a constant gear  $g^{(q)}$ , which represents the strength of the muscle, i.e.,

$$\tau_n^{(q)} = g^{(q)} \sigma_n^{(q)}. \quad (3)$$

Since the actions  $a_n^{(q)}$  are assumed to lie within the unit interval  $[-1, 1]$ , the gears determine the magnitude of applied torques. Details on the derivation of the gears are given in the Methods section below.

We learn a control policy using a motor babbling approach based on reinforcement learning. In this approach, the policy initially generates random movements, which are

rewarded with the negative time to reach randomly placed 3D targets of varying size with the right index finger. This reward signal implies movement time minimization for aimed movements. The policy is updated using the *soft-actor-critic* algorithm (SAC) [7]. The actor and critic networks both consist of two fully connected layers with 256 neurons each, followed by the output layer, which either returns the means and standard deviations of the action distributions (for the actor network) or the state-action value (for the critic network). The fully observable state includes among others the angles and velocities of all joints, as well as the target position. To make reinforcement learning computationally feasible, a fast physics simulation is necessary. Therefore, we implemented the above biomechanical model in MuJoCo [8].

It is important to note here that the assumption of minimizing total movement time does not provide any gradient to the reinforcement learner. In particular, it is not possible to distinguish beneficial states and actions from inappropriate ones before the target has been reached, which terminates the episode and thus increases the total return. This, together with the fairly small subspace of appropriate actions relative to the number of possible control vectors, makes it very difficult to obtain a reasonable policy without additional aid. For this reason, we created an adaptive curriculum, which dynamically decreases the target width from 60cm to less than 2cm diameter during training. This has shown to be both effective (targets with diameter around 2cm are consistently reached by the final policy) and efficient (this minimum width was reached after 1.2M steps, while various predetermined curricula required more than 3M steps).

## Results

### Fitts' Law

For evaluation of the trajectories resulting from our final policy for different target conditions, we designed a discrete Fitts' Law type task. The task follows the ISO 9241-9 ergonomics standard and incorporates 13 equidistant targets arranged in a circle at 50cm distance in front of the body and placed 10cm right of the right shoulder (Fig 2). The objective is for the end-effector to reach each target and to stay inside the target for 100ms. Although not included in the training phase, staying inside the target seemed to be no problem during evaluation. If both requirements are satisfied or 1.5 seconds have passed, the next target is given to the learned policy.

The Index of Difficulty (ID) of the tasks ranges from 1 to 4, where ID is computed as  $\log_2(D/W + 1)$ .  $D$  denotes the distance between initial and target position and  $W$  is the target size. We execute 50 movements for each task condition and each direction, i.e., 6500 movements in total. All of them were successful, i.e., the end-effector stayed inside the target for 100ms within the given 1.5 seconds.

Using the trajectories from this discrete pointing task, we evaluate whether the synthesized movements follow Fitts' Law [1], i.e., whether there exists a linear relationship between task difficulty (ID) and the required movement time. Fig 3 shows the total duration for each movement sorted by ID. The median movement times for each ID (green lines) are approximated by a linear function (red line, with  $R^2 = 0.9986$ ). This indicates that Fitts' Law holds for aimed movements simulated by the model.

### 2/3 Power Law

The 2/3 Power Law [2, 4, 9, 10] describes a relationship between the radius of curvature of the movement  $\rho_n$  and the corresponding velocity  $v_n$ :

$$v_n = k\rho_n^{1-\beta}, \tag{4}$$

$$\beta \approx 2/3, \tag{5}$$

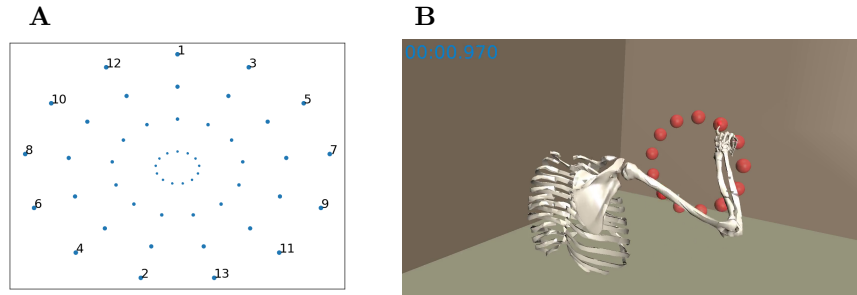


**Fig 2. ISO 9241-9 task.** **A:** The target setup in the discrete Fitts' Law type task. Different circles correspond to different IDs and distances between targets. **B:** Visualization of our biomechanical model performing aimed movements. Note that at each time step, only the *current* target (position and radius) is given to the learned policy.

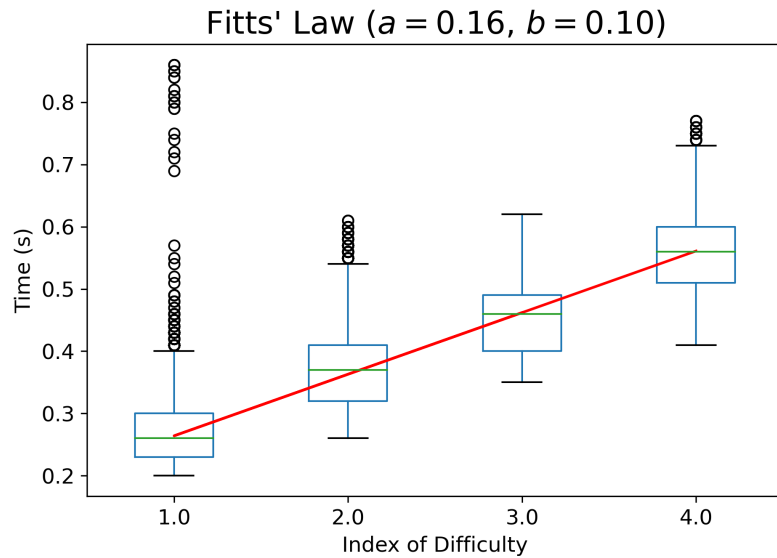


**Fig 3. Fitts' Law.** The movements generated by our learned policy follow Fitts' Law. Here, movement time is plotted against ID for all distances and IDs in the considered ISO task (6500 movements in total).

where the parameter  $k$  determines the velocity gain. We evaluate whether our model exhibits the  $2/3$  Power Law using an elliptic via-point task.

We define an ellipse in 2D space (55cm in front, 10cm above, and 10cm right of the shoulder) that completely lies within the area used for target sampling during training (ellipse radii are 7.5cm (horizontal) and 3cm (vertical)). Using the via-point method described in the Methods section below, our learned policy is used to trace the ellipse for 60 seconds as fast as possible (see Fig 4A). For the resulting trajectory, we compute  $\rho_n$  and  $v_n$  at all time steps sampled at a rate of 100Hz and then perform a log-log regression on these values. This gives us the optimal parameter values  $\beta = 0.65$  and  $k = 0.54$ , which suggests that the  $2/3$  Power Law holds. Both the data points and the linear approximation in log-log space are shown in Fig 4B.



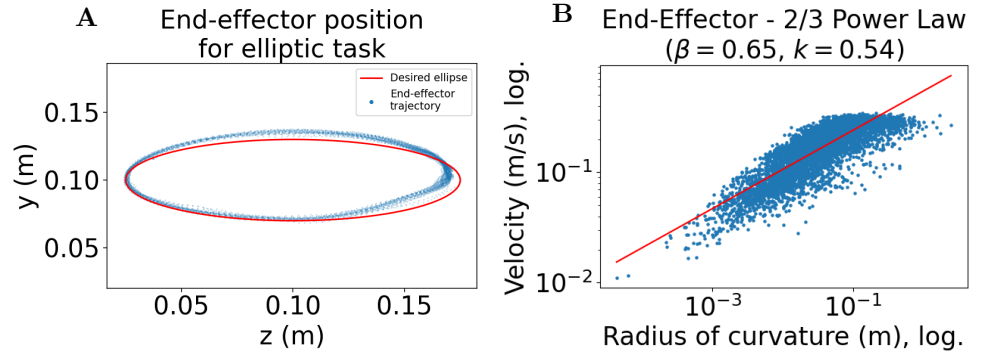


**Fig 4.  $2/3$  Power Law.** Elliptic movements generated by our learned policy follow the  $2/3$  Power Law.

**A:** End-effector positions projected into the 2D space (blue dots), where targets were subsequently placed along an ellipse of 15cm width and 6cm height (red curve).

**B:** Log-log regression of velocity against radius of curvature for end-effector positions sampled with 100Hz when tracing the ellipse for 60 seconds.

## Movement trajectories

In addition to Fitts' Law and the  $2/3$  Power Law, we qualitatively analyze the movement trajectories generated by the model. Figures 5 and 6 show position, velocity, and acceleration time series as well as 3D movement path, Phasespace, and Hooke plots for multiple movements from the Fitts' Law type task for two representative task conditions (ID 4 respective ID 2, each with 35cm distance between targets) and one representative movement direction (between targets 7 and 8 shown in Fig 2A). Apart from the 3D movement path, all plots show centroid projections of the respective trajectory onto the vector between initial and target position.

The movements exhibit typical features of human aimed movements, such as symmetric bell-shaped velocity profiles. Movements are smooth and gently accelerate and decelerate as visible in the acceleration profile and Hooke plot. For high ID (Fig 5), movements exhibit an initial rapid movement towards the target, followed by an extended phase of corrective movements. For low ID (Fig 6), the phase of corrective movements is generally shorter.

Movement trajectories towards the target are slightly curved and some of them exhibit pronounced correctional submovements at the end (see, e.g., S1 Fig and S2 Fig).

The between-movement variability within one movement direction and task condition decreases with increasing ID; in particular, very simple ID 1 movements exhibit a large variability and are most prone to outliers (see, e.g., S3 Fig).

For a few movement directions (mostly in ID 2 tasks), the corresponding plots seem to incorporate two different types of trajectories (see, e.g., S6 Fig): While some movements start with zero or even negative acceleration and show a typical N-shaped acceleration profile, others exhibit a positive acceleration at the beginning and their first peak is less pronounced. The reason for this behavior are corrective submovements at the end of the previous movement (see, e.g., S4 Fig and S5 Fig)<sup>1</sup>, leading to a different initial acceleration of the beginning of the subsequent movement. Apart from these notable features, almost all movements exhibit bell-shaped velocity and N-shaped acceleration profiles, as it is typical for pointing tasks [11].

<sup>1</sup>Note that in the Fitts' Law type task, the end-effector needs to stay inside the target for 100ms to successfully terminate the episode. If the target is left earlier, another attempt has to be made within the permitted total duration of 1.5s.

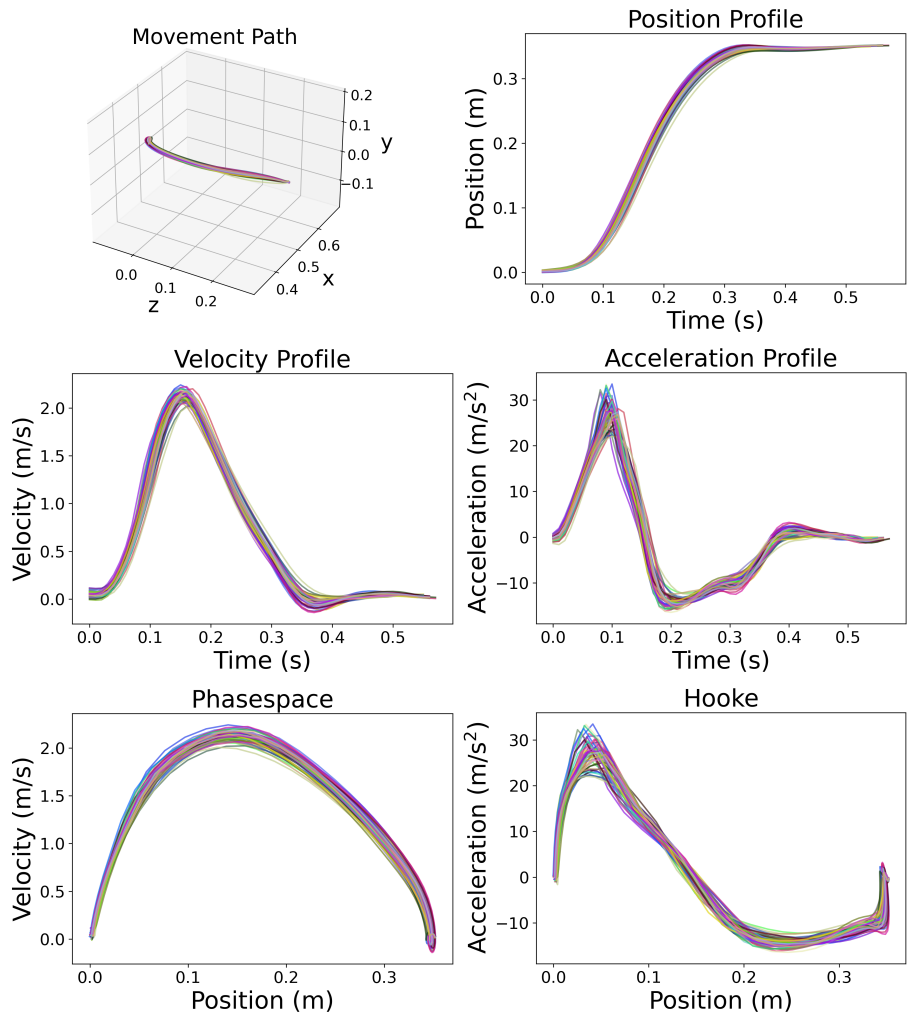


**Fig 5. End-effector trajectories (ID 4).** 3D path, projected position, velocity, acceleration, phasespace, and Hooke plots of 50 aimed movements (between targets 7 and 8 shown in Fig 2A) with ID 4 and a target distance of 35cm.

## Discussion

In summary, we can conclude that, under the assumption of movement time minimization given signal-dependent and constant motor noise, movement of the human upper extremity model produced by reinforcement learning follows both Fitts' Law and the  $2/3$  Power Law. Moreover, the generated trajectories exhibit features typical for pointing tasks, such as bell-shaped velocity and N-shaped acceleration profiles, and corrective submovements that increase with task difficulty. To our knowledge, this has not yet been shown for state-of-the-art biomechanical models of the upper extremity. This result supports the idea that the control of the complex human biomechanical system is plausible to be determined by a set of simple assumptions and can be easily learned.

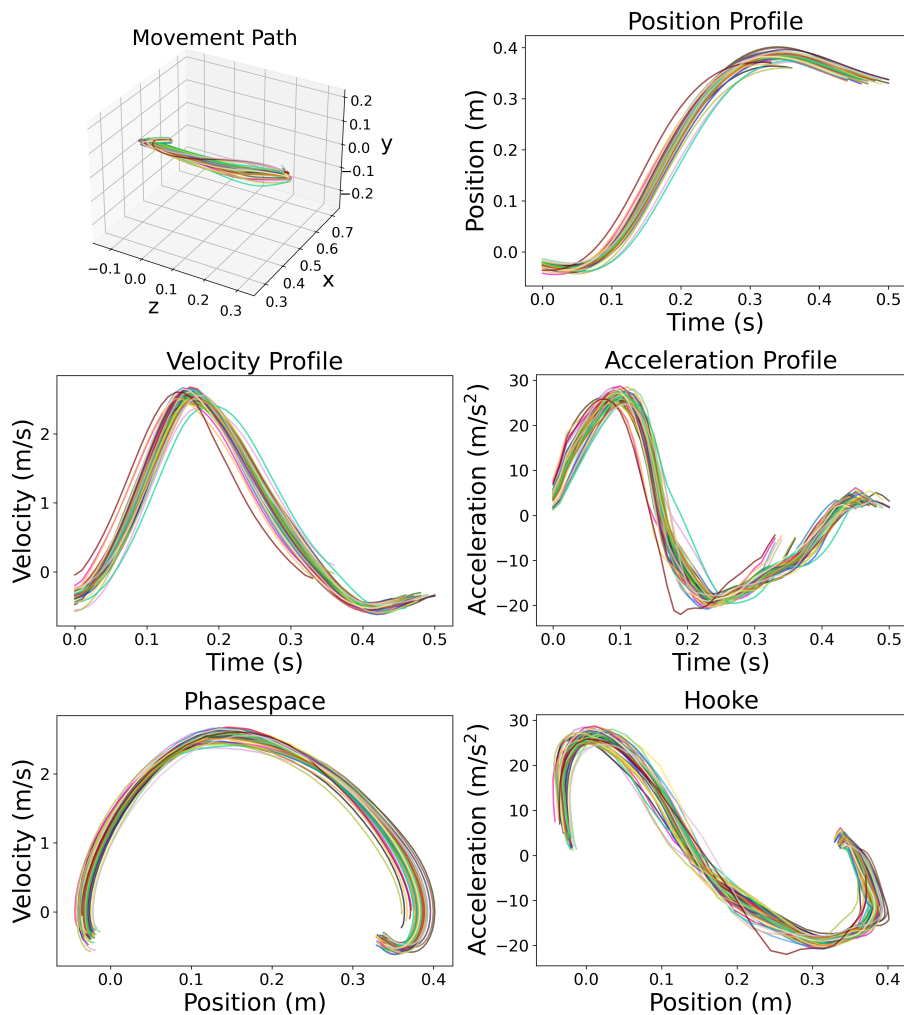


**Fig 6. End-effector trajectories (ID 2).** 3D path, projected position, velocity, acceleration, phasespace, and Hooke plots of 50 aimed movements (between targets 7 and 8 shown in Fig 2A) with ID 2 and a target distance of 35cm.

## Methods

In the following, we first describe the general reinforcement learning approach and give details about the underlying biomechanical model. Afterwards, we focus on individual components of our method, namely states, actions, gears, rewards, and an adaptive target selection mechanism. We also provide details about the implementation of our algorithm. Finally, we discuss the methods used for evaluation.

## Reinforcement Learning

We define the task of controlling the biomechanical model of the human upper extremity through motor control signals applied at the joints as a reinforcement learning problem, similar to [12]. In this formulation, a policy  $\pi_{\theta}(a|s)$  models the conditional distribution over actions  $a \in A$  (motor control signals applied at the individual DOFs) given the state  $s \in S$  (the pose, velocities, distance to target, etc.). The subindex  $\theta$  denotes the

parameters of the neural networks. At each timestep  $n \in \{0, \dots, N\}$ , we observe the current state  $s_n$  and sample a new action  $a_n$  from the current policy  $\pi_\theta$ . The physical effects of that action, i.e., the application of these motor control signals, constitute the new state  $s_{n+1}$ , which we obtain from our biomechanical simulation. We compute a reward  $r_n$  at each time step  $n$ , which allows to penalize the total time needed to reach a given target. The sum of the (discounted) rewards appears in the expected return

$$J(\theta) = \mathbb{E}_{\mathcal{T} \sim p_\theta(\mathcal{T})} \left[ \sum_{n=0}^N \gamma^n r_n \right], \quad (6)$$

which we want to maximize with respect to the parameters  $\theta$ , i.e., the goal is to learn the optimal parameters  $\theta^*$  that maximize  $J(\theta)$ . Here,

$$p_\theta(\mathcal{T}) = p(s_0) \prod_{n=0}^{N-1} \pi_\theta(a_n | s_n) p(s_{n+1} | s_n, a_n) \quad (7)$$

is the distribution over all possible trajectories  $\mathcal{T} = (s_0, a_0, \dots, a_{N-1}, s_N)$  induced by the policy  $\pi_\theta$ , while  $p(s_0)$  denotes the distribution of the initial states. In our model, given  $s_n$  and  $a_n$ , the subsequent state  $s_{n+1}$  is not deterministic, since both signal-dependent and constant noise are included (details are given in the Introduction). The probability of reaching some subsequent state  $s_{n+1} \in \mathcal{S}$  is thus given by  $p(s_{n+1} | s_n, a_n)$ . However, to our knowledge, there is no closed formula for  $s_{n+1}$ .<sup>2</sup> Hence, we cannot directly compute the expected value in Eq (6). Instead, we rely on sampling to approximate it. The total return of a trajectory is given by  $\sum_{n=0}^N \gamma^n r_n$ , where  $\gamma \in ]0, 1]$  is a discount factor that causes the learner to prefer earlier rewards over later rewards.

In order to approximate the optimal parameters  $\theta^*$ , we use a policy-gradient approach, which iteratively refines the parameters  $\theta$  in the direction of increasing rewards. Reinforcement learning methods that are based on fully sampled trajectories usually suffer from updates with high variance. To reduce this variance and thus speed up the learning process, we choose an approach that includes two approximators: an *actor network* and a *value network*. These work as follows: Given some state  $s_0$  as input, the actor network outputs the (standardized) mean and standard deviation of as many normal distributions as dimensions of the action space. The individual action components are then sampled from these distributions. To update the actor network weights, we require some measurement of how “desirable” some state  $s_0$  is, i.e., how much reward can be expected when starting in this state following the current policy. These values are given by the *state value function*<sup>3</sup>, which is defined as the expected sum of discounted rewards:

$$V(s_0) = \mathbb{E}_{a_n \sim \pi(s_n)} \left[ \sum_{n=0}^N \gamma^n r_n \right]. \quad (8)$$

The output of the value network is an approximation of this state value function.

These two networks are then coupled with the *soft actor-critic (SAC)* algorithm [7], which has been successfully used in physics-based character motion [13]: As a policy-gradient method, it can be easily used with a continuous action space such as continuous motor signals – something that is not directly possible with value function methods such as *DQN* [14]. As an off-policy method that makes use of a replay buffer,

<sup>2</sup>Even if the stochastic noise was omitted, the underlying dynamics would be too complex to yield an analytical solution.

<sup>3</sup>Note that given the current policy  $\pi_\theta$ ,  $V(s_0)$  corresponds to  $J(\theta)$  for some fixed initial state  $s_0$ .

it is quite sample-efficient, which is important since running forward physics simulations in MuJoCo constitutes the major part of the training duration. Moreover, it has been shown that SAC outperforms other state-of-the-art algorithms such as PPO [15] or TD3 [16]<sup>4</sup>. In order to obtain an unbiased estimate of the optimal value function, we use *Double Q-Learning* [17], using a separate target critic network. The neural network parameters are optimized using the Adam optimizer [18].

## Biomechanical Model of the Human Upper Extremity

Our biomechanical model of the human upper extremity is based on the *Upper Extremity Dynamic model* [5], which was originally implemented in *OpenSim* [19]. Kinematically, the model represents the human shoulder and arm using 7 physical bodies and 5 "phantom" bodies to model the complex movement of the shoulder. This corresponds to 3 joints (shoulder, elbow, and wrist) with 7 DOFs and 5 additional joints with 13 associated components coupled by 13 constraints with the DOFs. Each DOF has constrained joint ranges (see Table 1), which limits the possible movements. In contrast to linked-segment models, the *Upper Extremity Dynamic model* represents both translational and rotatory components of the movement within shoulder, clavicle, and scapula, and also within the wrist. It also contains physiological joint axis orientations instead of the perpendicular orientations in linked-segment models. The dynamics components of the musculoskeletal model are represented by the weight and inertia matrix of each non-phantom body and the default negligible masses and inertia of all phantom bodies. The dynamics properties of the model were extracted from multiple previously published works on human and cadaveric studies. The active components of the *Upper Extremity Dynamic Model* consist of 31 Hill-type muscles as well as of 14 coordinate limit forces softly generated by the ligaments when a DOF approaches the angle range limit. Further details of this model are given in [5].

**Table 1. Joint ranges of individual DOFs.**

Joint DOF	Joint Angle Ranges (deg)		Joint Torque Ranges (Nm)	
	Minimum	Maximum	Minimum	Maximum
elevation angle	-90	130	-36.01	36.01
shoulder elevation	0	180	-60.97	60.97
shoulder rotation	-90	20	-19.37	19.37
elbow flexion	0	130	-12.57	12.57
pronation/supination	-90	90	-1.03	1.03
wrist deviation	-10	25	-2.14	2.14
wrist flexion	-70	70	-1.53	1.53

Angle and torque ranges of all joint DOFs, which are actuated via second-order muscle dynamics (Eq 1). Gears are defined as the magnitude of the torque range limits.

In order to make reinforcement learning feasible, we manually implement the *Upper Extremity Dynamic Model* in the fast MuJoCo physics simulation [8]. With respect to kinematics, the MuJoCo implementation of the model is equivalent to the original OpenSim model and contains physiologically accurate degrees of freedom as well as corresponding constraints. We use the physiological masses of individual segments in the MuJoCo model. However, we compute the inertial properties using the geometry and density of model segments in MuJoCo instead of the inertia matrices from the

<sup>4</sup>Supporting the observations in [7], we also found our training process to be faster and more robust when using SAC compared to PPO.

OpenSim model. We do not implement muscles in the MuJoCo model, as this would significantly slow down the simulation and make reinforcement learning computationally infeasible due to the *curse of dimensionality*.<sup>5</sup> Instead, we implement simplified actuators, representing aggregated muscle action on each individual DOF, which are controlled using the second-order dynamics introduced in [21] with fixed time constants  $t_e = 30\text{ms}$  and  $t_a = 40\text{ms}$ . A formula of the discrete-time implementation used in our algorithm is given in Eq 1. We select the gears, and respectively the maximum torques for the actuators given in Table 1, based on experimental data as described in the subsequent section. We currently do not model the soft joint ranges in MuJoCo, as the movements the model produces to not usually reach joint limits.

Our biomechanical model provides the following advantages over simple linked-segment models:

- phantom bodies and joints allow for more realistic movements, including both translation and rotation components within an individual joint,
- individual joint angle and torque limits are set for every DOF,
- axes between joints are specifically chosen and not just perpendicular between two segments,
- the model includes physiological body segment masses, and it yields
- better options for scaling individual body parts, e.g., based on particular individuals.

## States, Actions, and Gears

Using the MuJoCo implementation of our biomechanical model described above, the **states**  $s \in \mathcal{S} \subseteq \mathbb{R}^{48}$  in our RL approach include the following information:

- joint angle for each DOF  $q \in \mathcal{Q}$  in radians (7 values),
- joint velocity for each DOF  $q \in \mathcal{Q}$  in radians/s (7 values),
- activations  $\sigma^{(q)}$  for each DOF  $q \in \mathcal{Q}$ , and their derivatives  $\dot{\sigma}^{(q)}$  ( $2 \times 7$  values),
- positions of the end-effector and target sphere ( $2 \times 3$  values),
- (positional) velocities of the end-effector and target sphere ( $2 \times 3$  values),
- (positional) acceleration of the end-effector (3 values),
- *difference vector*: vector between the end-effector attached to the index finger and the target, pointing towards the target (3 values),
- projection of the end-effector velocity towards the target (1 value),
- radius of the target sphere (1 value).

Each component  $a^{(q)} \in [-1, 1]$  of the **action vector**  $a = (a^{(q)})_{q \in \mathcal{Q}} \in \mathcal{A}$  is used to actuate some DOF  $q \in \mathcal{Q}$  by applying the torque  $\tau^{(q)}$  resulting from Eq 1-3. Note that in addition to these actuated forces, additional active forces (e.g., torques applied to parent joints) and passive forces (e.g., gravity and contact forces) act on the joints in every time step.

<sup>5</sup>In particular, computing dynamic actuator lengths (which significantly affect the forces produced by muscle activation patterns) has still proven challenging in MuJoCo [20].

We determine the maximum torque a human would exert at each DOF in this task experimentally as follows. We implemented the Fitts’ Law task described above in a VR environment displayed via the HTC Vive Pro VR headset. We recorded the movements of a single participant performing the task using the Phasespace X2E motion capture system<sup>6</sup> with a full-body suit provided with 14 optical markers. Using OpenSim, we scaled the *Upper Extremity Dynamic Model* to this particular person. We then used OpenSim to perform *Inverse Dynamics* to obtain the torque sequences that are most likely to produce the recorded marker trajectories. For each DOF  $q \in \mathcal{Q}$ , we set the corresponding **gear**  $g^{(q)}$  to the absolute maximum torque applied at this DOF during the experiment.<sup>7</sup> The resulting values are shown in Table 1.

## Reward Function and Curriculum Learning

The behavior of the policy is largely determined by the reward  $r_n$  that appears in (6) and (8). We designed the reward following Harris and Wolpert [4], who argue that there is no rational explanation why the central nervous system (CNS) should explicitly try to minimize previously proposed metrics such as the change in the torque applied at the joints [22], or the acceleration (or jerk) of the end-effector [23]. They argue that it is not even clear whether the CNS is able to compute, store, and integrate these quantities while executing motions.

Instead, they propose that the CNS aims to minimize movement end-point variance given a fixed movement time, under the constraint of signal-dependent noise. This is equivalent to minimizing movement time when the permissible end-point variance is given by the size of the target [4]. The equivalent objective is simple and intuitively plausible, since achieving accurate aimed movements in minimal time is critical for the success of many movement tasks.

Therefore, the objective of our model is *minimization of movement time while reaching a target of a given width*.

More precisely, our **reward function** only consists of a time reward, which penalizes every time step of an episode equally:

$$r_n = -100\Delta t. \tag{9}$$

This term provides incentives to terminate the episode (which can only be achieved by reaching the target) as early as possible. Since we apply each control  $a_n$  for 10ms,  $\Delta t$  amounts to 0.01 in our case, i.e.,  $r_n = -1$  for every time step  $n \in \{0, \dots, N\}$ .

According to our experience, it is possible to learn aimed movements despite the lack of gradient provided by the reward function, as long as a few requirements are met: The initial posture needs to be sampled randomly and the targets need to be large enough at the beginning of the training to ensure that the target is often enough reached by exploration in early training steps to guide the reinforcement learner. However, creating a predetermined curriculum that gradually decreases the target width during training appropriately has proved very difficult: In most cases, the task difficulty either increased too fast, leading to unnatural movements that do not reach the target directly (and often not at all), or progress was slow, resulting in a time-consuming training phase.

For this reason, we decided to use an adaptive curriculum, which dynamically adjusts the target width depending on the recent success rate. Specifically, we define a *curriculum state*, which is initialized with an initial target diameter of 60cm. Every 10K update steps, the current policy is evaluated on 30 complete episodes, where target diameters are chosen depending on the current state of the curriculum. Based on the

<sup>6</sup><https://www.phasespace.com/x2e-motion-capture/>

<sup>7</sup>We removed a small number of outliers, which we defined as values with distance to mean larger than 20 times the standard deviation.

percentage of targets reached within the permitted 1.5 seconds (*success rate*), the curriculum state is updated: If the success rate falls below 70%, it is increased by 1cm; if the success rate exceeds 90%, it is decreased by 1cm.<sup>8</sup>

At the beginning of each episode, the target diameter is set to the current curriculum state with probability  $1 - \varepsilon$ , and sampled uniformly random between 0.1cm and 60cm with probability  $\varepsilon = 0.1$ , which has proven to be a reasonable choice. This particularly ensures that all required target sizes occur throughout the training phase, and thus prevents forgetting how to solve “simpler” tasks (in literature often referred to as *catastrophic forgetting*; see, e.g., [24]).

## Implementation of the Reinforcement Learning Algorithm

The actor and critic networks described in the Reinforcement Learning section consist of two fully connected layers with 256 neurons each, followed by the output layer, which either returns the means and standard deviations of the action distributions (for the actor network) or the state-action value (for the critic network). To improve the speed and stability of learning, we train two separate, but same-structured critic networks and use the minimum of both outputs as the teaching signal for all networks (*Double Q-Learning*) [7, 17]. In all networks, ReLU [25] is used as non-linearity for both hidden layers.

The reinforcement learning methods of our implementation are based on the *TF-Agents* library [26]. The learning phase consists of two parts, which are repeated alternately: *trajectory sampling* and *policy updating*.

In the trajectory sampling part, the target position is sampled from the uniform distribution on a cuboid of 70cm height, 40cm width, and 30cm depth, whose center is placed 50cm in front of the human body and 10cm to the right of the shoulder. The width of the target is controlled by the adaptive curriculum described above. The biomechanical model is initialized with some random posture, where the joint angles are uniformly sampled from the convex hull of static postures that allow to keep the end-effector in one of 12 targets placed along the vertices of the above described cuboid. The initial joint velocities are uniformly sampled from the interval  $[-0.005 \text{ radians/s}, 0.005 \text{ radians/s}]$ .

In every step  $n \in \{0, \dots, N - 1\}$ , given the current state vector  $s_n \in \mathcal{S}$  (see description above), an action is sampled from the current policy  $\pi_\theta(s_n)$ . Next, the MuJoCo simulation uses this action to actuate the model joints, updates the body posture, and returns both the reward  $r_n$  and the subsequent state vector  $s_{n+1}$ . In our implementation, every episode in the learning process contains at most  $N = 100$  of such steps, with each step corresponding to 10ms.<sup>9</sup> If the target is reached earlier, i.e., the distance between end-effector and target center is lower than the radius of the target sphere, the current episode terminates and the next episode begins with new target position and width. At the beginning of the training, 10K steps are taken and the corresponding transitions are stored in a replay buffer, which has a capacity of 1M steps. During training, only one step is taken and stored per sampling phase.

In the policy updating part, 256 previously sampled transitions  $(s_n, a_n, r_n, s_{n+1})$  are randomly chosen from the replay buffer to update both the actor network and the critic network weights. We use a discount factor of 0.99 in the critic loss function of SAC. All other parameters are set to the default values of the TF-Agents SAC implementation [26].

<sup>8</sup>We clipped the resulting value to the interval  $[0.1\text{cm}, 60\text{cm}]$  to avoid target sizes that are larger than the initial width or are too close to zero.

<sup>9</sup>Allowing movements to be longer than one second did not improve the training procedure significantly.



Both parts of our learning algorithm, the trajectory sampling and the policy update, are executed alternately until the curriculum state, i.e., the current suggested target diameter, falls below 1cm.<sup>10</sup> To evaluate a policy  $\pi_\theta$ , we apply the action  $a_n^*$  with the highest probability under this policy at every time step (i.e., we use the corresponding *greedy* policy) and evaluate the resulting trajectory. Such an *evaluation* is done every 10K steps, where 30 complete episodes are generated using this deterministic policy, and resulting performance indicators are stored. After the training phase,  $\theta^*$  is set to the latest parameter set  $\theta$ , i.e., the final policy  $\pi_{\theta^*}$  is chosen as latest policy  $\pi_\theta$ .

An overview of the complete training procedure is given in Fig 7.

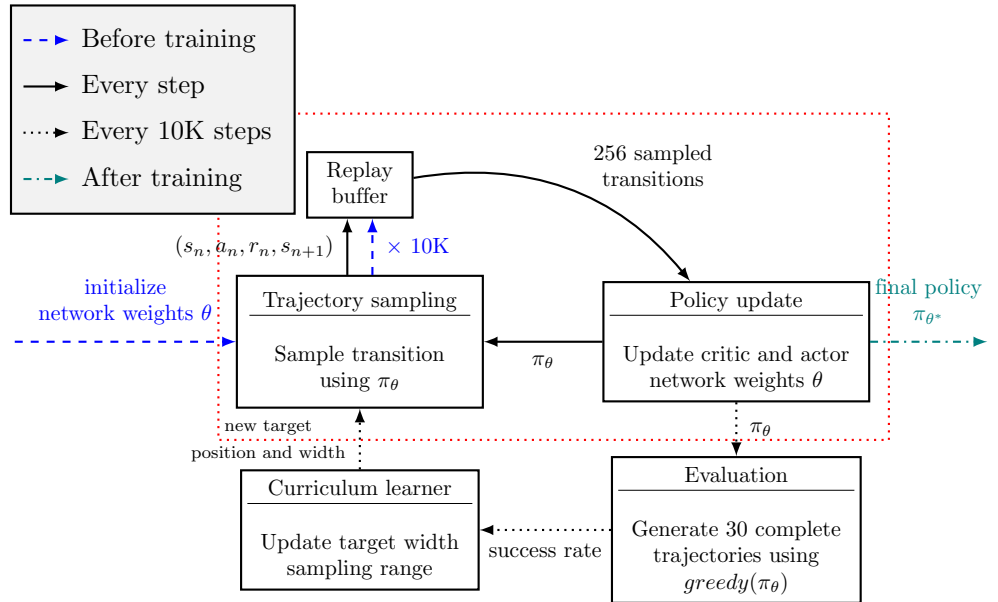


**Fig 7. Reinforcement learning procedure.** Before training, the networks are initialized with random weights, and 10K transitions generated using the resulting initial policy are stored in the replay buffer (blue dashed arrows). During training (red box), trajectory sampling and policy update steps are executed alternately in every step. The targets used in the trajectory sampling part are generated by the curriculum learner, which is updated every 10K steps based on an evaluation of the most recent (greedy) policy. As soon as the target width suggested by the curriculum learner falls below 1cm, the training phase is completed and the final policy is returned (teal dash-dotted arrow).

## Evaluation

For evaluation of the trajectories resulting from the learned policy for different target conditions, we designed a discrete Fitts’ Law type task. This task follows the ISO 9241-9 ergonomics standard and incorporates 13 equidistant targets arranged in a circle at 50cm distance in front of the body and placed 10cm right of the right shoulder (Fig 2). As soon as a target is reached and the end-effector stays inside for 100ms, the next target is given to the learned policy. This also happens after 1.5 seconds, regardless of whether the episode was successful.

Based on the recommendations in [27], we determine different task difficulty conditions by sampling “form and scale”, i.e., the *Index of Difficulty (ID)* and the distance  $D$  between the target centers are sampled independently instead of using a

<sup>10</sup>With our implementation, this was the case after 1.2M steps, corresponding to about 4 hours of training time.

distance-width grid. We use the *Shannon Formulation* [28] of Fitts’ Law to compute the resulting distance between initial and target point  $D$ , given the target width  $W$  and the ID:

$$\text{ID} = \log_2 \left( \frac{D}{W} + 1 \right). \quad (10)$$

The used combinations of distance, width, and ID are given in Table 2 and the resulting target setup is shown in Fig 2A.

**Table 2. Conditions in the Fitts’ Law Type Task.**

Distance $D$	Width $W$	ID
0.05	0.05	1
0.15	0.15	1
0.25	0.25	1
0.15	0.05	2
0.25	0.0833	2
0.35	0.1167	2
0.15	0.0214	3
0.25	0.0357	3
0.35	0.05	3
0.35	0.0233	4

Distance between initial point and target  $D$  (in meters), diameter of target sphere  $W$  (in meters), and resulting Index of Difficulty (ID) of task conditions used in the Fitts’ Law type task.

The model executes 50 movements for each task condition and each direction, i.e., 6500 movements in total. All movements reached the target and stayed inside for 100ms within the given maximum movement time of 1.5s. Plots for all task conditions and movement directions together with their underlying data can be found in a public repository [29].

In addition, an adaptive “moving target” mechanism is applied to generate elliptic movements from our learned policy. During training, the policy only has learned to reach a given target as fast and accurate as possible – it was never asked to follow a specific path accurately. For this reason, we make use of the following method:

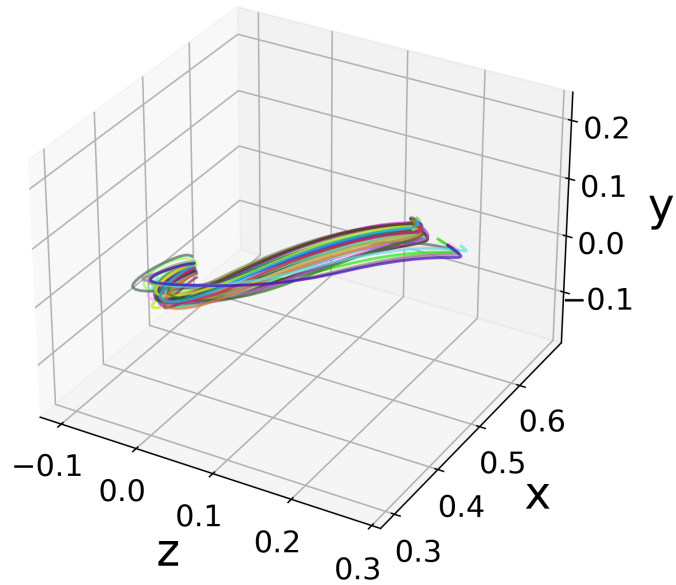
Initially, we place the first target on the ellipse such that 10% of the complete curve need to be covered clockwise within the first movement, starting in a fixed initial position (the leftmost point on the ellipse). In contrast to regular pointing tasks, the target already switches as soon as the movement (or rather the projection of the movement path onto the ellipse) covers more than half of this distance. The next target is then chosen to again create an incentive to cover the next 10% of the elliptic curve. Thus, there are roughly 20 via-points in total subsequently placed on the ellipse. As shown in Fig 4A, this indeed leads to fairly elliptic movements.

For our evaluation, we use an ellipse with horizontal and vertical diameter of 15cm and 6cm (similar to the ellipse used in [4]), with its center placed 55cm in front, 10cm above, and 10cm right of the shoulder. The task was performed for one minute, where end-effector position, velocity, and acceleration was stored every 10ms.

Comprehensive data for all of these movements can be found in [29].

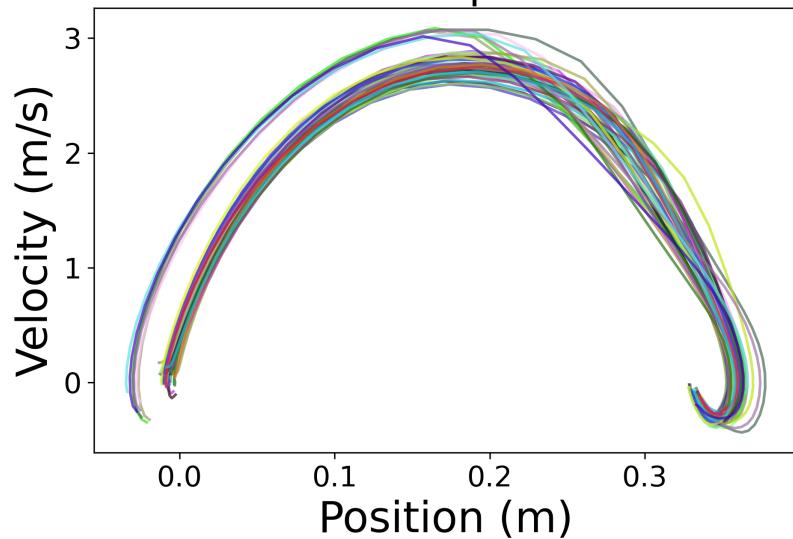
## Supporting information

### Movement Path

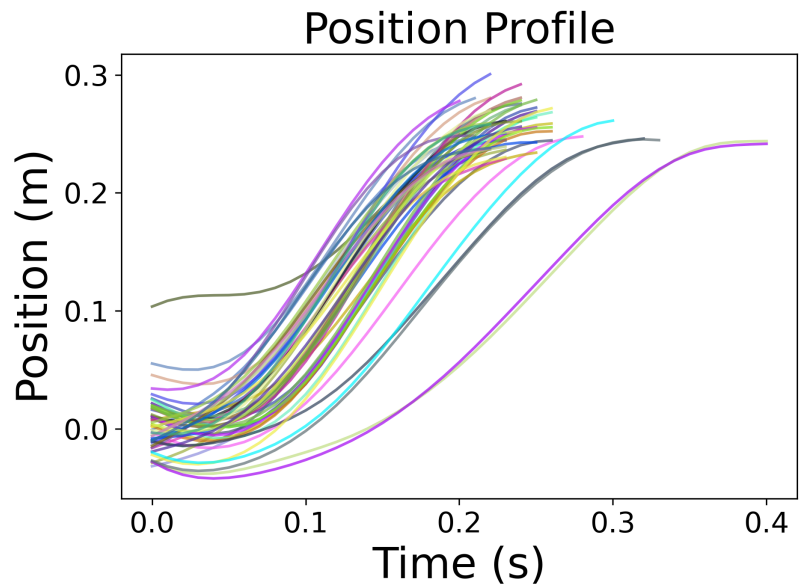


**S1 Fig. Movement with change of direction (3D Path).** For some trajectories, the direction changes towards the end of the movement (here: ID 2, 35cm distance, movements between targets 5 and 6).

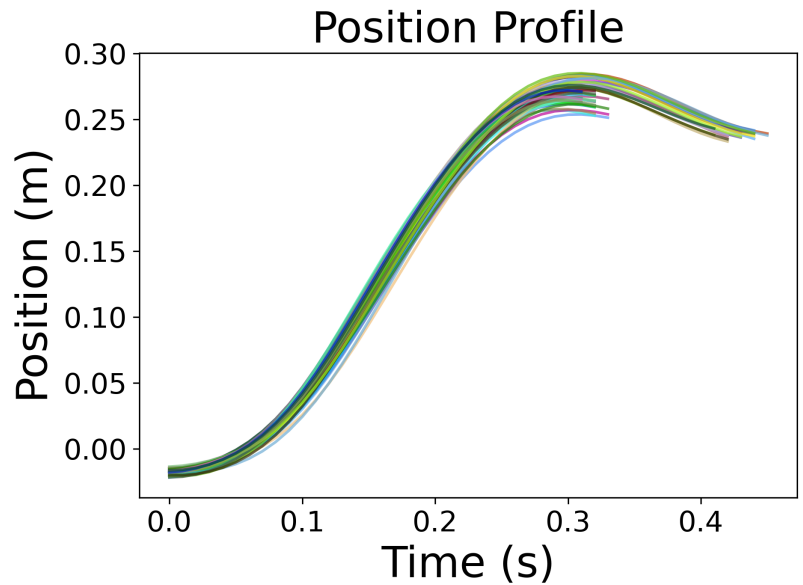
### Phasespace



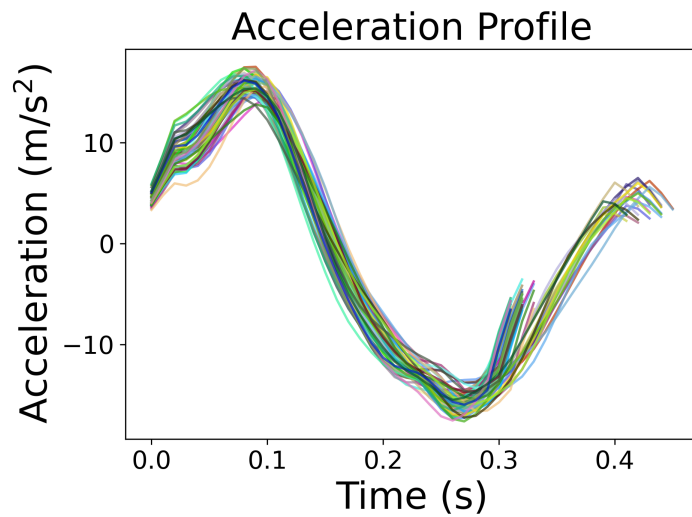
**S2 Fig. Movement with change of direction (Phasespace).** Changes of direction towards the end of a movement are also visible in the appendix at the right side of the Phasespace plot. (here: ID 2, 35cm distance, movements between targets 5 and 6).



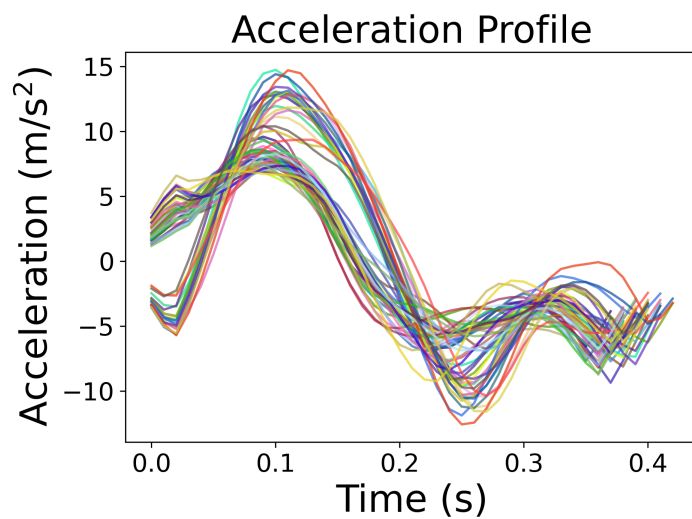
**S3 Fig. Trajectory variability in ID 1 movements (Position).** For simple ID 1 movements, the between-trial variability is the largest. In addition, some “outliers” with considerably higher reaction time might occur (here: ID 1, 25cm distance, movements between targets 1 and 2).



**S4 Fig. Corrective Submovements (Position).** For some trials, the end-effector does not stay inside the target for the required 100ms. A corrective submovement (here after 0.3s) then enables a second attempt (here: ID 2, 25cm distance, movements between targets 9 and 10).



**S5 Fig. Corrective Submovements (Acceleration).** For some trials, the end-effector does not stay inside the target for the required 100ms. A corrective submovement (here after 0.3s) then enables a second attempt (here: ID 2, 25cm distance, movements between targets 9 and 10).



**S6 Fig. Movements with different initial conditions (Acceleration).** The extent of corrective submovements in the previous movement (see S4 Fig and S5 Fig) determines the initial acceleration, which in turn affects the shape of, e.g., the acceleration profile (here: ID 2, 25cm distance, movements between targets 10 and 11).

## Acknowledgments

We would like to thank Aldo A. Faisal (Imperial College London) for his helpful comments on the manuscript.

## References

1. Fitts PM. The information capacity of the human motor system in controlling the amplitude of movement. *Journal of experimental psychology*. 1954;47(6):381.
2. Lacquaniti F, Terzuolo C, Viviani P. The law relating the kinematic and figural aspects of drawing movements. *Acta Psychologica*. 1983;54(1):115 – 130. doi:10.1016/0001-6918(83)90027-6.
3. Schaal S, Sternad D. Origins and violations of the 2/3 power law in rhythmic 3D movements. In: *Experimental Brain Research*. vol. 136; 2001. p. 60–72. Available from: <http://www-clmc.usc.edu/publications/S/schaal-EBR2001.pdf>.
4. Harris CM, Wolpert DM. Signal-dependent noise determines motor planning. *Nature*. 1998;394:780–4. doi:10.1038/29528.
5. Saul KR, Hu X, Goehler CM, Vidt ME, Daly M, Velisar A, et al. Benchmarking of dynamic simulation predictions in two software platforms using an upper limb musculoskeletal model. *Computer methods in biomechanics and biomedical engineering*. 2014;5842(May 2016):1–14. doi:10.1080/10255842.2014.916698.
6. van Beers RJ, Haggard P, Wolpert DM. The Role of Execution Noise in Movement Variability. *Journal of Neurophysiology*. 2004;91(2):1050–1063. doi:10.1152/jn.00652.2003.
7. Haarnoja T, Zhou A, Hartikainen K, Tucker G, Ha S, Tan J, et al.. *Soft Actor-Critic Algorithms and Applications*; 2018. Available from: <https://arxiv.org/abs/1812.05905>.
8. Todorov E, Erez T, Tassa Y. MuJoCo: A physics engine for model-based control. In: *2012 IEEE/RSJ International Conference on Intelligent Robots and Systems*; 2012. p. 5026–5033.
9. Viviani P, Schneider R. A developmental study of the relationship between geometry and kinematics in drawing movements. *Journal of experimental psychology Human perception and performance*. 1991;17 1:198–218.
10. Viviani P, Mounoud P. Perceptuomotor Compatibility in Pursuit Tracking of Two-Dimensional Movements. *Journal of Motor Behavior*. 1990;22(3):407–443. doi:10.1080/00222895.1990.10735521.
11. Abend W, Bizzi E, Morasso P. Human arm trajectory formation. *Brain: a journal of neurology*. 1982;105(Pt 2):331–348.
12. Cheema N, Frey-Law LA, Naderi K, Lehtinen J, Slusallek P, Hämäläinen P. Predicting Mid-Air Interaction Movements and Fatigue Using Deep Reinforcement Learning. In: *Proceedings of the 2020 CHI Conference on Human Factors in Computing Systems*. CHI '20. New York, NY, USA: Association for Computing Machinery; 2020. p. 1–13. Available from: <https://doi.org/10.1145/3313831.3376701>.
13. Peng XB, Abbeel P, Levine S, van de Panne M. DeepMimic: Example-Guided Deep Reinforcement Learning of Physics-Based Character Skills. *ACM Transactions on Graphics*. 2018;37(4):1–14. doi:10.1145/3197517.3201311.
14. Sutton RS, Barto AG. *Reinforcement Learning: An Introduction*. Cambridge, MA, USA: A Bradford Book; 2018.

15. Schulman J, Wolski F, Dhariwal P, Radford A, Klimov O. Proximal Policy Optimization Algorithms; 2017. Available from: <https://arxiv.org/abs/1707.06347>.
16. Fujimoto S, van Hoof H, Meger D. Addressing Function Approximation Error in Actor-Critic Methods; 2018. Available from: <https://arxiv.org/abs/1802.09477>.
17. Hasselt HV. Double Q-learning. In: Lafferty JD, Williams CKI, Shawe-Taylor J, Zemel RS, Culotta A, editors. Advances in Neural Information Processing Systems 23. Curran Associates, Inc.; 2010. p. 2613–2621. Available from: <http://papers.nips.cc/paper/3964-double-q-learning.pdf>.
18. Kingma DP, Ba J. Adam: A Method for Stochastic Optimization; 2014. Available from: <https://arxiv.org/abs/1412.6980>.
19. Delp SL, Anderson FC, Arnold AS, Loan P, Habib A, John CT, et al. OpenSim: Open-Source Software to Create and Analyze Dynamic Simulations of Movement. IEEE Transactions on Biomedical Engineering. 2007;54(11):1940–1950.
20. Ikkala A, Hämäläinen P. Converting Biomechanical Models from OpenSim to MuJoCo; 2020. Available from: <https://arxiv.org/abs/2006.10618>.
21. van der Helm FCT, Rozendaal LA. 11. In: Winters JM, Crago PE, editors. Musculoskeletal Systems with Intrinsic and Proprioceptive Feedback. New York, NY: Springer New York; 2000. p. 164–174. Available from: [https://doi.org/10.1007/978-1-4612-2104-3\\_11](https://doi.org/10.1007/978-1-4612-2104-3_11).
22. Uno Y, Kawato M, Suzuki R. Formation and Control of Optimal Trajectory in Human Multijoint Arm Movement - Minimum Torque-Change Model. Biological cybernetics. 1989;61:89–101. doi:10.1007/BF00204593.
23. Flash T, Hogan N. The Coordination of Arm Movements: An Experimentally Confirmed Mathematical Model. Journal of neuroscience. 1985;5:1688–1703.
24. McCloskey M, Cohen NJ. Catastrophic Interference in Connectionist Networks: The Sequential Learning Problem. In: Bower GH, editor. Psychology of Learning and Motivation. vol. 24. Academic Press; 1989. p. 109 – 165. Available from: <http://www.sciencedirect.com/science/article/pii/S0079742108605368>.
25. Nair V, Hinton GE. Rectified Linear Units Improve Restricted Boltzmann Machines. In: Proceedings of the 27th International Conference on International Conference on Machine Learning. ICML'10. Madison, WI, USA: Omnipress; 2010. p. 807–814.
26. Sergio Guadarrama, Anoop Korattikara, Oscar Ramirez, Pablo Castro, Ethan Holly, Sam Fishman, Ke Wang, Ekaterina Gonina, Neal Wu, Efi Kokiopoulou, Luciano Sbaiz, Jamie Smith, Gábor Bartók, Jesse Berent, Chris Harris, Vincent Vanhoucke, Eugene Brevdo. TF-Agents: A library for Reinforcement Learning in TensorFlow; 2018. <https://github.com/tensorflow/agents>. Available from: <https://github.com/tensorflow/agents>.
27. Guiard Y. The Problem of Consistency in the Design of Fitts' Law Experiments: Consider Either Target Distance and Width or Movement Form and Scale. In: Proceedings of the SIGCHI Conference on Human Factors in Computing Systems. CHI '09. New York, NY, USA: Association for Computing Machinery; 2009. p. 1809–1818. Available from: <https://doi.org/10.1145/1518701.1518980>.

28. MacKenzie IS. A Note on the Information-Theoretic Basis for Fitts' Law. *Journal of Motor Behavior*. 1989;21(3):323–330. doi:10.1080/00222895.1989.10735486.
29. Fischer F, Bachinski M, Klar M, Fleig A, Müller J. Reinforcement Learning Control of a Biomechanical Model of the Upper Extremity; 2020. Dataset on Zenodo. Available from: <https://dx.doi.org/10.5281/zenodo.4268230>.